

Article

Design of a Port-Hamiltonian Control for an Alt-Azimuth Liquid-Mirror Telescope

Juan Cristobal Alcaraz Tapia ¹, Carlos E. Castañeda ^{1,*}, Héctor Vargas Rodríguez ¹ and P. Esquivel ²

¹ Universidad de Guadalajara, Centro Universitario de los Lagos, Lagos de Moreno 47460, Mexico; cristobal.alcaraz@alumnos.udg.mx (J.C.A.T.); hector.vrodriguez@academicos.udg.mx (H.V.R.)

² CONAHCYT-Universidad Autónoma de Tamaulipas, Ciudad Victoria 87000, Mexico; pesquivelpr@conahcyt.mx

* Correspondence: carlose.castanedah@academicos.udg.mx

Abstract: In this work, we design a control strategy to be applied in a port-Hamilton representation of a liquid-mirror telescope for an alt-azimuth configuration. Starting from a dynamical model for an alt-azimuth liquid-mirror telescope based on Lagrange mechanics, a transformation to the port-Hamilton form is made. Such a dynamical model is obtained by computing the kinetic and potential energy of the telescope and substituting them in the Euler–Lagrange equation of motion. Then, for the transformation to the port-Hamiltonian form, we obtain the relation between the Hamiltonian and the Lagrangian. The resulting open-loop model based on the Hamiltonian function is controlled using an extension of the interconnection and damping-assignment passivity-based control aiming for a robust and accurate steady behavior in the closed loop while tracking a star’s position. For comparison purposes, two different control strategies are applied to the Lagrangian model, inverse-dynamics control and sliding mode super-twisting control. Since the light is collected by the principal mirror of the telescope while tracking a star, we make a description of the liquid mirror’s behavior. The tracking star’s position is described as a function of the observer’s position and the star’s coordinates as well as the date of observation. The simulations’ results show that the port-Hamilton control has a good transitory and steady response as well as great accuracy competing with that of inverse-dynamics control but with greater robustness and no chattering drawback.

Keywords: port-Hamiltonian control; liquid mirror; alt-azimuth telescope; star tracking

MSC: 70H03; 70H05; 70H14; 93B12; 93B17; 93B18; 93C10; 93D09; 93D15; 93D30



Citation: Alcaraz Tapia, J.C.; Castañeda, C.E.; Vargas Rodríguez, H.; Esquivel, P. Design of a Port-Hamiltonian Control for an Alt-Azimuth Liquid-Mirror Telescope. *Mathematics* **2023**, *11*, 3443. <https://doi.org/10.3390/math11163443>

Academic Editors: Yuri Vladimirovich Mitrishkin and Nikolay M. Kartsev

Received: 10 June 2023
Revised: 1 August 2023
Accepted: 2 August 2023
Published: 8 August 2023



Copyright: © 2023 by the authors. Licensee MDPI, Basel, Switzerland. This article is an open access article distributed under the terms and conditions of the Creative Commons Attribution (CC BY) license (<https://creativecommons.org/licenses/by/4.0/>).

1. Introduction

Liquid-mirror telescopes use a rotating fluid as their principal mirror; with this, there is no need either for the precise process of polishing or shaping the principal mirror because a rotating fluid adopts naturally the required shape (parabola) for a Newtonian principal mirror. Furthermore, the bigger a principal mirror is the more complex and robust its bearing needs to be to reduce its deformation, thus elevating its cost. In this regard, a liquid-mirror telescope can be built at a fraction of the cost of a conventional telescope of similar sizes, such as the case of the 6 m Large Zenith Telescope [1]. However, due to the nature of the rotating fluid, its container has to stand vertical and cannot be tilted; therefore, liquid-mirror telescopes are fixed to observe only the zenith and cannot track any object in the sky [2,3]. So, liquid-mirror telescopes are only used for specific types of tasks, where it is sufficient to analyze just the sky above the observer or for tasks where it does not matter what portion of the sky is being observed; for instance, the 4 m International Liquid-Mirror Telescope [4] was built to carry out astrometric observations of the solar system, galactic and extra-galactic objects within a 24’ strip of sky, aiming to detect quasars and supernovas.

For a telescope to be able to track any star in the sky, it needs to be set on a mount that can rotate around two different axes. This configuration resembles that of a manipulator

robot and a basic control for a manipulator is the inverse-dynamics control (IDC) which cancels nonlinearities via feedback linearization. For general nonlinear systems, such feedback linearization may be quite difficult or impossible to achieve, but for the particular case of a manipulator robot model, the design of this control is actually easy. Nevertheless, such a control algorithm requires that the parameters of the system are known exactly to achieve the exact cancellation of nonlinearities [5,6].

In contrast to the IDC, the sliding-mode control is a strategy that is robust against model uncertainties and external disturbances [7], meaning that it does not require an exact model of a plant to perform good tracking and it can even reject external forces acting on the plant, so it can keep the tracking, but it has the known chattering drawback. Hence, some strategies have been developed to reduce the chattering, one of them is the super-twisting algorithm [7–11]. Nevertheless, according to authors in [12], the super-twisting algorithm implies a non-Lipschitzian function with infinite derivative at the origin in addition to a discontinuous input function, resulting in two sources of chattering instead of one as is the case for conventional sliding-mode control. Its chattering amplitude becomes higher than that of the conventional one as the value of the unmodeled dynamic increases.

In nonlinear systems, the port-Hamilton paradigm has attracted attention since the closed-loop preserves the port-Hamilton structure. Thus, it exploits the intrinsic properties of the system rather than trying to impose some predetermined dynamic behavior through the cancellation of nonlinearities and high gain (used in robust control techniques) [13]. One of the control algorithms developed for a port-controlled Hamiltonian (PCH) system is the interconnection and damping-assignment passivity-based control (IDA-PBC), a well-documented method where a storage function, representing the total energy of the system, can be shaped so the minimum state of energy is the desired equilibrium. Then, that equilibrium is reached by injecting damping into the system. This control strategy allows for an energy interpretation of the control action enhancing the physical intuition, because this energy approach of the port-Hamiltonian framework serves as a *lingua franca* for the different domains of a multi-domain physical system, facilitating the communication of control theorists and practitioners that are familiar with energy concepts [14].

Since the introduction of the PCH strategy [15,16], many applications have been reported in the literature, including mechanical systems [17–20]. Nevertheless, the original IDA-PBC strategy was designed aiming for regulation and not for tracking, so for this work, we apply an extension proposed by [21] that can track a desired feasible trajectory, preserving the port-Hamiltonian structure in a closed loop. This control strategy for the PCH system is to be compared with the IDC and the sliding-mode control. Summarizing, each one of these controllers has a different approach to deal with nonlinearities; the IDC cancels the nonlinearity by means of feedback linearization, compensating for the nonlinearity [5]; the sliding-mode control is used to dominate the effect of model uncertainties, designing a sliding manifold that is independent of model uncertainties, such that the trajectories on the manifold converge to the equilibrium point [22]; the control developed for the PCH does not cancel or dominate nonlinearities, but exploits the intrinsic properties of the system, leading to a nonlinear closed-loop structure where the passivity plays a central role, achieving stabilization by rendering the system passive with respect to a desired storage function and injecting damping [13]. In addition to the mentioned strategies, if the complexity of a system is high, due to nonlinearities, external disturbances or uncertainties in the model, a reasonable alternative is a fuzzy logic approach, such as that proposed in [23], which is robust against time-varying disturbances and independent of system dynamics, although it is not a simple controller.

This work presents the design and synthesis of a port-Hamiltonian control algorithm of a liquid-mirror telescope for an alt-azimuth configuration which is considered as a two-degrees-of-freedom robot arm. This is done by obtaining the open-loop representation of the Port-Hamiltonian model using the Lagrangian function associated with the telescope. By means of the interconnection of a damping-assignment passivity-based control, the closed-loop of the port-Hamiltonian representation is designed, where it is possible to

track variant signals, which represent the trajectory of the specific stars. The performance results of the port-Hamiltonian control algorithm are compared with the super-twisting and inverse dynamics ones with the aim of obtaining in the sense of tracking the *Regulus* star at a specific latitude and date.

The main contribution of this work is to obtain a port-Hamiltonian representation of an alt-azimuth liquid-mirror telescope considered a two-degrees-of-freedom robot arm. A closed-loop Hamiltonian control algorithm is designed and synthesized to track the trajectory of any specific star and the observer can see the star at any latitude.

This work is organized as follows: Section 2 shows the most important information to describe the technical issues used in this work; in Section 3, the proposed methodology is presented to show the steps for designing and synthesizing the three controllers; in Section 3.7, the simulation results are depicted and the performance of the controllers designed in this work is shown; finally, the conclusions are presented in Section 4.

2. Background

This section describes the IDA-PBC technique, starting from the general form that a system must adopt before we can apply this technique, until the differences with the extension allow us to track a trajectory. As we are comparing the PCH system with other controllers, this section also presents the general theory of the super-twisting sliding-mode control algorithm.

2.1. General Form of a Port-Hamilton System

It is known that the general form of a port-controlled Hamiltonian (PCH) model in input–output form is as follows [14]:

$$\Sigma := \begin{cases} \dot{x} = [J(x) - R(x)] \frac{\partial \mathcal{H}}{\partial x} + [g(x)]u, & x \in \mathcal{X}, u \in \mathbb{R}^m \\ y = [g(x)]^\top \frac{\partial \mathcal{H}}{\partial x}, & y \in \mathbb{R}^m \end{cases} \quad (1)$$

where x is the state vector, \mathcal{X} is an n -dimensional state space manifold, the Hamiltonian $\mathcal{H}(x) : \mathbb{R}^n \rightarrow \mathbb{R}$ represents the total stored energy, u is the input and (u, y) are the power variables—the product $u^\top y$ represents the power flows exchanged with the environment of the system. The interconnection structure is captured by the $n \times n$ interconnection matrix $J(x) = -J^\top(x)$ that is skew symmetric and by the $n \times m$ matrix $g(x)$; the $n \times n$ damping matrix $R(x) = R^\top \geq 0$ is positive semi-definite; the superscript (\top) represents the transposed matrix or vector.

A control scheme that exploits the port-Hamilton structure is the interconnection and damping-assignment passivity-based control (IDA-PBC) introduced in [16]. For physical systems, the designer can adjust the energy exchange and dissipation of the system through the interconnection and damping matrices, respectively. We can state the main proposition of IDA-PBC as follows [13]:

Theorem 1 (IDA-PBC). Consider system (1); assume that there are matrices $g^\perp(x)$, $J_d(x) = -J_d^\top(x)$, $R_d(x) = R_d^\top \geq 0$ and a function $\mathcal{H}_d : \mathbb{R}^n \rightarrow \mathbb{R}$ that verify the Partial Differential Equation:

$$g^\perp(x)[J(x) - R(x)] \frac{\partial \mathcal{H}}{\partial x} = g^\perp(x)[J_d(x) - R_d(x)] \frac{\partial \mathcal{H}_d}{\partial x}, \quad (2)$$

where $g^\perp(x)$ is a full-rank left annihilator of $g(x)$, i.e., $g^\perp(x)g(x) = 0$, and $\mathcal{H}_d(x)$ is such that:

$$x_* = \arg \min \mathcal{H}_d(x), \quad (3)$$

where x_* in \mathbb{R}^n is the equilibrium to be stabilized. Then, closed-loop system (1), with $u = \beta(x)$, where

$$\beta(x) = [g^\top(x)g(x)]^{-1}g^\top(x) \left\{ [J_d(x) - R_d(x)] \frac{\partial \mathcal{H}_d}{\partial x} - [J(x) - R(x)] \frac{\partial \mathcal{H}}{\partial x} \right\}, \tag{4}$$

takes the following PCH form:

$$\dot{x} = [J_d(x) - R_d(x)] \frac{\partial \mathcal{H}_d}{\partial x}, \tag{5}$$

where x_* is a (locally) stable equilibrium. It will be asymptotically stable if, in addition, x_* is an isolated minimum of $\mathcal{H}_d(x)$ and the largest invariant set under the closed-loop dynamics (5) contained in

$$\left\{ x \in \mathbb{R}^n \mid \frac{\partial \mathcal{H}_d}{\partial x}^\top R_d(x) \frac{\partial \mathcal{H}_d}{\partial x} = 0 \right\}, \tag{6}$$

equals $\{x_*\}$.

Since the priority of the aforementioned control is regulation and not tracking, we use an extension of this control for tracking proposed in [21] with the following theorem:

Theorem 2 (tIDA-PBC). Consider $x^*(t)$ as a feasible trajectory of system (1) with $J_d = -J_d^\top$, $R_d = R_d^\top \geq 0$. Suppose that $A_d = J_d - R_d$ is a Hurwitz matrix, D_0 is an open subset of \mathbb{R}^n and there exist positive constants $0 \leq \alpha_1 \leq \alpha_2$ such that $\mathcal{H} : \mathbb{R}^n \times \mathbb{R} \rightarrow \mathbb{R}$ satisfies the following condition:

$$\alpha_1 I \leq \nabla^2 \mathcal{H}_d(x, t) \leq \alpha_2 I, \forall x \in D_0, \tag{7}$$

and the following matching equation:

$$g^\perp(x)[J(x) - R(x)] \frac{\partial \mathcal{H}}{\partial x}(x) = g^\perp(x)[J_d - R_d] \frac{\partial \mathcal{H}_d}{\partial x}(x, t), \tag{8}$$

where g^\perp is the full-rank left annihilator of g . If J_d, R_d and \mathcal{H}_d satisfy the following equation (the closed-loop system evaluated at $x^*(t)$):

$$\dot{x}^*(t) = (J_d - R_d) \frac{\partial \mathcal{H}_d}{\partial x}(x^*(t), t), \tag{9}$$

then, there exists a controller in the form of:

$$u = (g^\top(x)g(x))^{-1}g^\top(x) \left((J_d - R_d) \frac{\partial \mathcal{H}_d}{\partial x}(x, t) - (J(x) - R(x)) \frac{\partial \mathcal{H}}{\partial x}(x) \right), \tag{10}$$

When Equation (10) is substituted in system (1), it makes it locally an exponential tracker for $x^*(t)$ and causes the closed-loop system to have the following form:

$$\begin{aligned} \dot{x} &= [J(x) - R(x)] \frac{\partial \mathcal{H}}{\partial x} + [g(x)](g^\top(x)g(x))^{-1} \\ &\quad g^\top(x) \left((J_d - R_d) \frac{\partial \mathcal{H}_d}{\partial x}(x, t) - (J(x) - R(x)) \frac{\partial \mathcal{H}}{\partial x}(x) \right) \\ &= (J_d - R_d) \frac{\partial \mathcal{H}_d}{\partial x}(x, t). \end{aligned} \tag{11}$$

It is to be noted that the general solution for the matching Equation (8) is in the form $\mathcal{H}_d(x) = \mathcal{H}(x) + \mathcal{H}_a$, where $\mathcal{H}_a = h_1(x) + \frac{1}{2}K(h_2(x) - L)^2$, and $h_1(x)$ and $h_2(x)$ are known functions, $K > 0$ is a proportional gain matrix and L is assigned such that condition (9) is satisfied.

2.2. Super-Twisting Sliding-Mode Control

The very well-known super-twisting sliding-mode control algorithm constitutes a decent robust strategy for controlling non-linear systems such that the control signal becomes a continuous time function due to it being inserted as an integrator into the control loop [7]. This control algorithm is a very good strategy for reducing the chattering effect and results in a quasi-continuous control signal.

For this, we consider that the non-linear mathematical model to be controlled has the following generic form:

$$\begin{aligned} \dot{x} &= f(x, t) + E(x, t)u(t) + \varphi(x, t), \\ y &= x_1, \end{aligned} \tag{12}$$

where $x = [x_1, x_2, \dots, x_n]^T \in X \subset \mathbb{R}^n$ is the state space vector consisting of r blocks; for the function vector $f(x, t) = [f_1(x_1, t), f_2(x_2, t), \dots, f_n(x_n, t)]^T, f : [0, \infty) \times D \rightarrow \mathbb{R}^n$ is piecewise continuous in t and Locally Lipschitz in x on $[0, \infty) \times D \subset \mathbb{R}^n$, which is a domain that contains the origin $x = 0$ [24], with $i = 1, 2, \dots, n$; the columns of matrix E are smooth and $\text{rank}(E(x, t)) = m$. The unknown mapping $\varphi(x, t)$ represents the external disturbances $d(t)$ and parameter variations; $u(t)$ is the control input vector bounded by:

$$0 \leq u(t) \leq u_{max}, \text{ for all } t > 0. \tag{13}$$

The value u_{max} corresponds to the maximum input value delivered by the source and $y = x_1$ is the output of the system. We use the procedure for designing the sliding manifold by transforming non-linear system (12) to the non-linear block controllable form based on the error dynamics. Then, the transformed system of the mathematical model to be controlled has the following general form:

$$\begin{aligned} \dot{z}_i &= -k_i z_i + E_1 z_{i+1} + \hat{\varphi}_i(z_i), \\ \dot{z}_r &= \bar{f}_r(z, x_{id}, \dot{x}_{id}, t) + \bar{E}_r(z)u + \bar{\varphi}_r(z), \end{aligned} \tag{14}$$

where $i = 1, \dots, r - 1; z_i = x_i - x_{id} = [z_i, \dots, z_{r-1}]^T$ which represents the i -th error vector, with the subscript d as the desired state value; the gains k_i are the components of the diagonal matrix K which is Hurwitz and guarantees the convergence of the closed-loop system.

Proposition 1. *The non-linear system with general form (12) can be transformed to the desired block control form based on dynamics error (14), where $\bar{f}_r(z, x_{id}, \dot{x}_{id}, t)$ is a bounded function and $\text{rank}(\bar{E}_r) = m$.*

The proof of Proposition 1 is presented in [25].

Once the plant to be controlled with the general form (12) is transformed in dynamics error (14), the sliding manifold can be selected as $s_D = z_r$ and the sliding mode $s_i = 0$, the error vector $z_i = x_{ref,i} - x_i$ and in its time derivative \dot{z}_r (second equation of system (14)) are obtained; then, the super-twisting control algorithm can be applied as follows (as explained in [26]):

$$v_s = \lambda |s|^{\frac{1}{2}} \text{sign } s + v_{s1}, \tag{15}$$

where $\dot{v}_s = \alpha_i \text{sign } s, \lambda = \begin{bmatrix} \lambda_\alpha & 0 \\ 0 & \lambda_\beta \end{bmatrix}$ and $\alpha = \begin{bmatrix} \alpha_\alpha & 0 \\ 0 & \alpha_\beta \end{bmatrix}$. For simplicity, the procedure for selecting the diagonal matrices λ_i and α_i is not shown and the reader is kindly referred to [26]. Therefore, the sliding surface s_D converges to the origin in finite time and the following new system is obtained:

$$\begin{aligned} \dot{s}_i &= F_i(\lambda_r, z_1, s) - E_2 \left(\lambda |s|^{\frac{1}{2}} \text{sign } s + v_{s1} \right), \\ \dot{v}_{s1} &= \alpha \text{sign } s. \end{aligned} \tag{16}$$

2.3. Dynamical Model of the Liquid-Mirror Telescope

The dynamics of the proposed alt-azimuth liquid-mirror telescope is developed as that of a manipulator comprised of two perpendicular links. Each link has an independent movement corresponding to one of the two coordinates of a star’s position.

The kinematics of the telescope depends on its geometric configuration, which describes the relative position of each link with respect to another and with respect to an inertial frame (0-frame (x_0, y_0, z_0)); these frames are depicted in Figure 1. The 1-frame (x_1, y_1, z_1) and 2-frame (x_2, y_2, z_2) are fixed to the telescope’s 1-link and 2-link, respectively. The orientation of the telescope is determined by the generalized coordinates q_1 and q_2 , with q_1 rotating about the z_0 axis and q_2 about the z_1 axis. Notice that the unseen axes perpendicular to the paper are determined by the right-hand rule; then, for example, axis x_1 is pointing towards the reader.

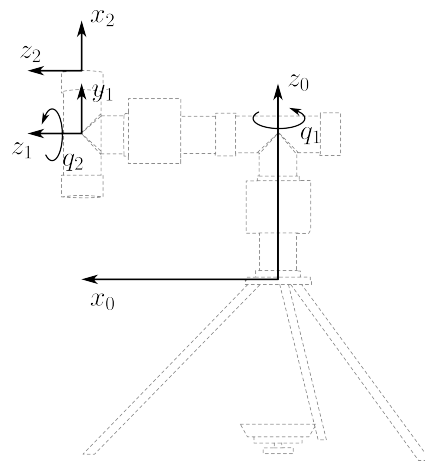


Figure 1. Position and orientation of the inertial frame and the body fixed frames of the proposed alt-azimuth liquid-mirror telescope.

The development of the telescope’s dynamical model is based on its potential and kinetic energy. Since the rotation of q_1 does not change the elevation of any link, its potential energy depends only on the value of q_2 . For the kinetic energy, we need to know the linear and angular velocities of each link in a common frame. This can be done with the aid of homogeneous transformations $T \in SE(3)$, which have the following form [5]:

$$T_{(\xi,\lambda,q_i)} = \begin{bmatrix} H_{(\xi,q_i)} & d \\ \mathbf{0} & 1 \end{bmatrix}; \quad H \in SO(3), \quad d \in \mathbb{R}^3, \quad (17)$$

where the $H_{(\xi,q_i)}$ matrix represents the rotation in an angle q_i about the axis defined by the unit vector ξ and d is a vector with magnitude λ in the ξ direction; it represents the relative position. We define the translation matrix $Trans_{(\xi,\lambda)} = T_{(\xi,\lambda,0)}$ and the rotation matrix as $Rot_{(\xi,q_i)} = T_{(\xi,0,q_i)}$.

Then, from Figures 1 and 2, we can compute the relative position and orientation of the 1-frame with respect to the 0-frame with consecutive transformations ($Trans, Rot \in SE(3)$)

$$T_1^0 = Trans_{(z,B_1)} Rot_{(z,q_1)} Trans_{(x,l_1+B_2)} Rot_{(y,\frac{\pi}{2})} Rot_{(z,\frac{\pi}{2})}, \quad (18)$$

$$T_1^0 = \begin{bmatrix} -\sin(q_1) & 0 & \cos(q_1) & (l_1 + B_2) \cos(q_1) \\ \cos(q_1) & 0 & \sin(q_1) & (l_1 + B_2) \sin(q_1) \\ 0 & 1 & 0 & B_1 \\ 0 & 0 & 0 & 1 \end{bmatrix}.$$

Equation (18) can be interpreted as if the 1-frame and the 0-frame start overlapped; then, the 1-frame is translated along its z axis a distance B_1 ($Trans_{(z,B_1)}$); then, it is rotated

about the z axis a variable angle q_1 ($Rot_{(z,q_1)}$); then, it is translated along its x axis a distance $l_1 + B_2$ ($Trans_{(x,l_1+B_2)}$), and so on.

The relation between the 2-frame and the 1-frame is obtained in a similar way as:

$$T_2^1 = Rot_{(z,q_2)} Trans_{(x,l_2)},$$

$$T_2^1 = \begin{bmatrix} \cos(q_2) & -\sin(q_2) & 0 & l_2 \cos(q_2) \\ \sin(q_2) & \cos(q_2) & 0 & l_2 \sin(q_2) \\ 0 & 0 & 1 & 0 \\ 0 & 0 & 0 & 1 \end{bmatrix}. \tag{19}$$

Now, the relation of the 2-frame with respect to the 0-frame is computed with a simple relation $T_2^0 = T_1^0 T_2^1$.

Thus, the orientation of the 1-frame with respect to the 0-frame, for example, is obtained from the first three rows and columns of (18) as:

$$H_1^0 = \begin{bmatrix} -\sin(q_1) & 0 & \cos(q_1) \\ \cos(q_1) & 0 & \sin(q_1) \\ 0 & 1 & 0 \end{bmatrix}, \tag{20}$$

and the position of its origin is determined by the first three elements of the last column. The relative orientation and position of the 2-frame with respect to the 0-frame (H_2^0) are extracted in a similar way from T_2^0 . Now, with the matrices H_1^0 and H_2^0 , it is possible to transform any vector in the 1-frame and 2-frame to the inertial frame (0-frame); even the constant inertia tensors in each fixed frame can be described in the inertial frame. Hence, we can sum the linear and angular velocities provided by each link in a common frame to compute the kinetic energy. Also, we can adjust the transformations (18) and (19) to represent the position vector of each link’s center of mass in the inertial frame, to compute the potential energy.

2.3.1. Kinematics

The alt-azimuth liquid-mirror telescope prototype comprises two links that rotate independently. The side view of this telescope is presented in Figure 2 and the corresponding parameters are shown in Table 1.

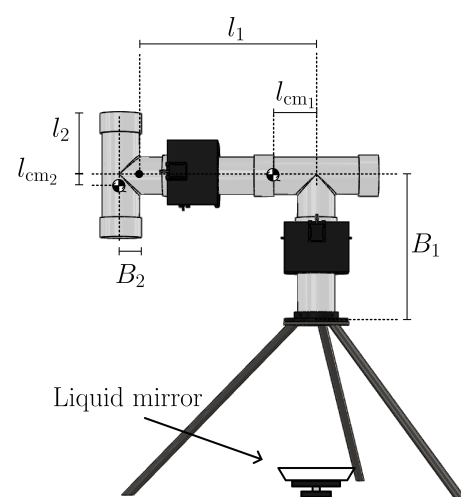


Figure 2. Side view of the alt-azimuth liquid-mirror telescope. The parameters are shown in Table 1.

Table 1. Parameters of the telescope.

Parameter	Value	Unit
m_1	6.360	kg
m_2	3.860	kg
l_1	0.400	m
l_2	0.190	m
l_{cm1}	0.080	m
l_{cm2}	−0.012	m
B_1	0.450	m
B_2	0.201	m
I_1	diag(0.340, 0.255, 0.105)	kg·m ²
I_2	diag(0.043, 0.061, 0.032)	kg·m ²

This configuration of the telescope allows us to conduct the light from a star, by using two plane mirrors, directly to a liquid mirror on the base, as it shows the direction of the yellow-dashed arrows presented in the cross-section of Figure 3. The liquid mirror will converge all the light towards its focus, where it can be collected by a CCD device.

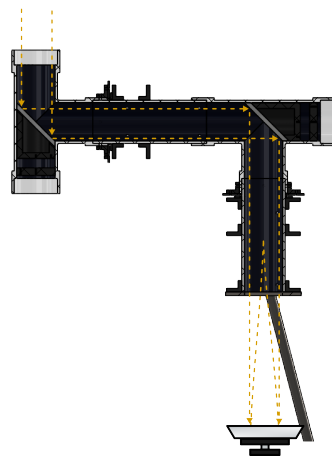


Figure 3. Cross-section view of the alt-azimuth liquid-mirror telescope. The yellow-dashed arrows represent light coming from a star conveyed to the liquid mirror at the base.

Now we can represent the position of the center of mass of each link for this configuration of the telescope. Using transformation (18), but changing the element $Trans_{x,l_1+B_2}$ by $Trans_{x,l_{cm_1}}$, we calculate the position of the 1-link center of mass instead of the origin of the 1-frame. Thus, from the resulting transformation, we obtain the following position vector relative to the x_0, y_0, z_0 set:

$$r_1 = \begin{bmatrix} l_{cm1} \cos q_1 \\ l_{cm1} \sin q_1 \\ B_1 \end{bmatrix}. \tag{21}$$

In a similar way, we can obtain the position vector for the 2-link’s center of mass relative to the x_0, y_0, z_0 set as:

$$r_2 = \begin{bmatrix} (l_1 + B_2) \cos q_1 - l_{cm2} \cos q_2 \sin q_1 \\ (l_1 + B_2) \sin q_1 + l_{cm2} \cos q_1 \cos q_2 \\ B_1 + l_{cm2} \sin q_2 \end{bmatrix}. \tag{22}$$

2.3.2. Potential and Kinetic Energy

The potential energy depends on the geometry of the telescope. For each link, its potential energy is written as follows:

$$\mathcal{U}_1 = m_1 g B_1, \tag{23}$$

$$\mathcal{U}_2 = m_2 g (B_1 + l_{cm_2} \sin q_2), \tag{24}$$

where the parameters m_i as the mass of the i -th link with $i = 1, 2$, B_1 are described in Table 1; l_{cm_2} is the 2-link's center of mass; g is the acceleration of gravity.

The total potential energy is:

$$\mathcal{U}(\mathbf{q}) = \mathcal{U}_1 + \mathcal{U}_2. \tag{25}$$

Before computing the kinetic energy, let us define first the Jacobians J_{vci} and J_{wi} and the inertia tensor I_i . From Figure 1, we can see the direction of the vectors z_0 and z_1 ; the first is represented with respect to the inertial frame, but the latter needs to be transformed by using the rotation matrix H_1^0 (20), resulting in $z_1^0 = H_1^0 z_1$; then we can define the 3×2 matrices J_{w_1} and J_{w_2} as:

$$J_{w_1} = [z_0^0 \quad 0] = \begin{bmatrix} 0 & 0 \\ 0 & 0 \\ 1 & 0 \end{bmatrix}, \quad J_{w_2} = [z_1^0 \quad z_0^0] = \begin{bmatrix} 0 & \cos(q_1) \\ 0 & \sin(q_1) \\ 1 & 0 \end{bmatrix}. \tag{26}$$

The 3×2 matrices J_{vc_1} and J_{vc_2} are defined as the partial derivative of r_1 (21) and r_2 (22) with respect to \mathbf{q} as follows:

$$J_{vc_1} = \begin{bmatrix} -l_{cm_1} \sin(q_1) & 0 \\ l_{cm_1} \cos(q_1) & 0 \\ 0 & 0 \end{bmatrix}, \tag{27}$$

$$J_{vc_2} = \begin{bmatrix} -\sin(q_1)(B_2 + l_1) - l_{cm_2} \cos(q_1) \cos(q_2) & l_{cm_2} \sin(q_1) \sin(q_2) \\ \cos(q_1)(B_2 + l_1) - l_{cm_2} \cos(q_2) \sin(q_1) & -l_{cm_2} \cos(q_1) \sin(q_2) \\ 0 & l_{cm_2} \cos(q_2) \end{bmatrix}, \tag{28}$$

where \mathbf{q} is the generalized coordinate (Euler angles) vector that indicates the orientation of the telescope with dimension two and which is defined as follows:

$$\mathbf{q} = [q_1 \quad q_2]^T. \tag{29}$$

We consider the inertia tensor of the i -th link evaluated around a frame parallel to the i -th frame but whose origin is at the center of mass and the principal axes are aligned to those of i -th frame; it is represented as:

$$I_i = \begin{bmatrix} I_{i_{xx}} & 0 & 0 \\ 0 & I_{i_{yy}} & 0 \\ 0 & 0 & I_{i_{zz}} \end{bmatrix}. \tag{30}$$

The kinetic energy for the two links of the telescope depends on both a translation term and a rotational term; this is computed as [5]:

$$\begin{aligned} \mathcal{K} &= \frac{1}{2} \dot{\mathbf{q}}^T \sum_{i=1}^n [m_i J_{vc_i}(\mathbf{q})^T J_{vc_i}(\mathbf{q}) + J_{w_i}(\mathbf{q})^T H_i^0(\mathbf{q}) I_i H_i^0(\mathbf{q})^T J_{w_i}(\mathbf{q})] \dot{\mathbf{q}} \\ &= \frac{1}{2} \dot{\mathbf{q}}^T D(\mathbf{q}) \dot{\mathbf{q}}, \end{aligned} \tag{31}$$

where $D(\mathbf{q})$ is called the inertia matrix of the system which is symmetric positive definite and for the proposed telescope this is written as:

$$D(\mathbf{q}) = \begin{bmatrix} \sigma_1 & -l_{cm_2} m_2 \sin(q_2) (B_2 + l_1) \\ -l_{cm_2} m_2 \sin(q_2) (B_2 + l_1) & m_2 l_{cm_2}^2 + I_{2_{zz}} \end{bmatrix}, \tag{32}$$

where $\sigma_1 = m_2(l_1 + B_2)^2 + m_1 l_{cm_1}^2 + (m_2 l_{cm_2}^2 - I_{2_{xx}} + I_{2_{yy}}) \cos(q_2)^2 + I_{1_{yy}} + I_{2_{xx}}$.

2.3.3. State-Space Model of the Telescope from Euler–Lagrange Equations

Since the telescope has the dynamics of a manipulator robot with two degrees of freedom, we can derive its dynamical model using the Euler–Lagrange equations of motion as follows [5]:

$$\frac{d}{dt} \frac{\partial \mathcal{L}}{\partial \dot{q}} - \frac{\partial \mathcal{L}}{\partial q} = \tau, \tag{33}$$

where $\tau = [\tau_1 \ \tau_2]^T$ is the vector of external torques and \mathcal{L} is the Lagrangian function defined as:

$$\mathcal{L}(q, \dot{q}) = \mathcal{K}(q, \dot{q}) - \mathcal{U}(q). \tag{34}$$

Then, the Lagrangian computed from Equations (25) and (31) is substituted into (33) to obtain the following matrix representation:

$$\begin{bmatrix} \tau_1 \\ \tau_2 \end{bmatrix} = D(q) \begin{bmatrix} \ddot{q}_1 \\ \ddot{q}_2 \end{bmatrix} + C(q, \dot{q}) \begin{bmatrix} \dot{q}_1 \\ \dot{q}_2 \end{bmatrix} + g(q), \tag{35}$$

where the matrix $D(q)$ is defined in (32) and the matrices $C(q, \dot{q})$ and $g(q)$ are:

$$C(q, \dot{q}) = \begin{bmatrix} -\dot{q}_2 \sin(2q_2) \left(m_2 l_{cm_2}^2 - I_{2_{xx}} + I_{2_{yy}} \right) & -\dot{q}_2 l_{cm_2} m_2 \cos(q_2) (B_2 + l_1) \\ \dot{q}_1 \sin(2q_2) \left(\frac{m_2 l_{cm_2}^2}{2} - \frac{I_{2_{xx}}}{2} + \frac{I_{2_{yy}}}{2} \right) & 0 \end{bmatrix}, \tag{36}$$

$$g(q) = \begin{bmatrix} 0 \\ 9.81 l_{cm_2} m_2 \cos(q_2) \end{bmatrix}. \tag{37}$$

Solving (35) for \ddot{q}_1 and \ddot{q}_2 , we can write a state–space model representation for the telescope as:

$$\begin{bmatrix} \dot{x}_1 \\ \dot{x}_2 \end{bmatrix} = \begin{bmatrix} x_3 \\ x_4 \end{bmatrix}, \tag{38}$$

$$\begin{bmatrix} \dot{x}_3 \\ \dot{x}_4 \end{bmatrix} = - \left[D^{-1}(x_1, x_2) \right] \left[C(x) \begin{bmatrix} x_3 \\ x_4 \end{bmatrix} + g(x_2) \right] + \left[D^{-1}(x_1, x_2) \right] \begin{bmatrix} \tau_1 \\ \tau_2 \end{bmatrix},$$

where the state vector is:

$$x^T = [x_1 \ x_2 \ x_3 \ x_4] = [q_1 \ q_2 \ \dot{q}_1 \ \dot{q}_2]. \tag{39}$$

It is important to mention that the dynamical model of the proposed alt-azimuth liquid-mirror telescope (38) is used for synthesizing the NBC-STSM and IDC algorithms. This is with the aim of comparing these algorithms with the PHC one.

3. Main Results

This section comprises the port-Hamilton representation of the proposed telescope’s dynamical model, the design of the IDA and the super-twisting sliding-mode controllers for the Euler–Lagrange representation model, the design of the control for the port-Hamilton representation, the obtaining of the trajectories that the telescope must track (star’s position) and the description of the liquid mirror’s shape. The reference signal to track is the star position represented by two coordinates corresponding to the rotation of each of the two links of the proposed telescope. With respect to the liquid mirror, this needs to adopt a specific shape by rotating its container; this relationship is also described.

3.1. Port-Hamiltonian Representation of the Telescope

The control strategy tIDA-PBC from Theorem 2 that is meant to control the telescope is designed to work on a model in the port-Hamiltonian representation (1) and the representation is dependent on the Hamiltonian function. Therefore, we start by computing the Hamiltonian. As stated in [27], its representation as a function of q and \dot{q} is as follows:

$$\mathcal{H}(q, \dot{q}) = \frac{\partial \mathcal{L}}{\partial \dot{q}} \dot{q} - \mathcal{L}(q, \dot{q}), \tag{40}$$

where $\frac{\partial \mathcal{L}}{\partial \dot{q}}$ is the generalized momentum p , which is defined as follows:

$$p = \frac{\partial \mathcal{L}}{\partial \dot{q}} = D(q)\dot{q}. \tag{41}$$

Then, the Hamiltonian can be written as a function of the independent variables q and p (notice that, from (41), in this case \dot{q} is considered a function of q and p), leading to the equation:

$$\mathcal{H}(q, p) = p^\top \dot{q} - \mathcal{L}(q, \dot{q}). \tag{42}$$

Therefore, solving (41) for \dot{q} and substituting it into (42) along with the Lagrangian \mathcal{L} , the Hamiltonian of the alt-azimuth telescope is:

$$\mathcal{H}(q, p) = \frac{1}{2} p^\top D^{-1}(q) p + g(B_1(m_1 + m_2) + m_2 l_{cm2} \sin(q_2)). \tag{43}$$

Now that the Lagrangian (34) and the Hamiltonian (43) for the telescope are defined and we know the relation of \mathcal{H} with \mathcal{L} and p with \dot{q} , as stated in [27], we can obtain the values for \dot{q} and \dot{p} . These values are obtained from Euler–Lagrange Equation (33) in terms of the Hamiltonian gradient ($\frac{\partial \mathcal{H}}{\partial x}$) and the external torques, that is:

$$\dot{q} = \frac{\partial \mathcal{H}}{\partial p}, \quad \dot{p} = -\frac{\partial \mathcal{H}}{\partial q} + \tau. \tag{44}$$

Since the Hamiltonian gradient is $\frac{\partial \mathcal{H}}{\partial x} = [\frac{\partial \mathcal{H}}{\partial q_1}, \frac{\partial \mathcal{H}}{\partial q_2}, \frac{\partial \mathcal{H}}{\partial p_1}, \frac{\partial \mathcal{H}}{\partial p_2}]^\top$, we can write (44) in the following form:

$$\begin{aligned} \begin{bmatrix} \dot{q} \\ \dot{p} \end{bmatrix} &= \begin{bmatrix} \mathbf{0} & \mathbf{I} \\ -\mathbf{I} & \mathbf{0} \end{bmatrix} \frac{\partial \mathcal{H}}{\partial x} + \begin{bmatrix} \mathbf{0} \\ \mathbf{I} \end{bmatrix} \tau, \\ y &= \begin{bmatrix} \mathbf{0} & \mathbf{I} \end{bmatrix} \frac{\partial \mathcal{H}}{\partial x}, \end{aligned} \tag{45}$$

where \mathbf{I} is a 2×2 identity matrix and $\mathbf{0}$ is a 2×2 zero matrix. From system (45), we can identify the following matrices:

$$J = \begin{bmatrix} \mathbf{0} & \mathbf{I} \\ -\mathbf{I} & \mathbf{0} \end{bmatrix}, \quad R = \begin{bmatrix} \mathbf{0} & \mathbf{0} \\ \mathbf{0} & \mathbf{0} \end{bmatrix}, \quad g = \begin{bmatrix} \mathbf{0} \\ \mathbf{I} \end{bmatrix}. \tag{46}$$

For a better visualization, compact representation (45) is expanded (using the values of Table 1) as follows:

$$\begin{bmatrix} \dot{q}_1 \\ \dot{q}_2 \\ \dot{p}_1 \\ \dot{p}_2 \end{bmatrix} = \begin{bmatrix} 0 & 0 & 1 & 0 \\ 0 & 0 & 0 & 1 \\ -1 & 0 & 0 & 0 \\ 0 & -1 & 0 & 0 \end{bmatrix} \begin{bmatrix} \frac{\partial \mathcal{H}}{\partial q_1} \\ \frac{\partial \mathcal{H}}{\partial q_2} \\ \frac{\partial \mathcal{H}}{\partial p_1} \\ \frac{\partial \mathcal{H}}{\partial p_2} \end{bmatrix} + \begin{bmatrix} 0 & 0 \\ 0 & 0 \\ 1 & 0 \\ 0 & 1 \end{bmatrix} \begin{bmatrix} \tau_1 \\ \tau_2 \end{bmatrix}, \tag{47}$$

$$\begin{bmatrix} y_1 \\ y_2 \end{bmatrix} = \begin{bmatrix} \frac{\partial \mathcal{H}}{\partial p_1} \\ \frac{\partial \mathcal{H}}{\partial p_2} \end{bmatrix},$$

where

$$\begin{bmatrix} \frac{\partial \mathcal{H}}{\partial q_1} \\ \frac{\partial \mathcal{H}}{\partial q_2} \\ \frac{\partial \mathcal{H}}{\partial p_1} \\ \frac{\partial \mathcal{H}}{\partial p_2} \end{bmatrix} = \begin{bmatrix} 0 \\ \cos(q_2)(0.186 \sin(q_2)\dot{q}_1^2 - 0.0278\dot{q}_1\dot{q}_2 - 0.4544) \\ \dot{q}_1 \\ \dot{q}_2 \end{bmatrix}.$$

The resulting equation, Equation (47), is the PCH model of the proposed telescope and, as it is in the form (1), we can apply the control strategy tIDA-PBC to track the trajectory of an arbitrary star using control law (10).

3.2. Port-Hamilton Control

To exploit the port-Hamilton structure, we use an extension of IDA-PBC for tracking, proposed in [21], since IDA-PBC originally is designed for regulation and not for tracking. The extension is called the tIDA-PBC control strategy and is described in Theorem 2. The desired control law (10) depends on the annihilator matrix (g^\perp), the desired interconnection matrix (J_d), the desired damping matrix (R_d) and the desired Hamiltonian (\mathcal{H}_d). All these elements are present in the matching Equation (8) and although they are described in Theorem 2, for clarity we are going to explain them again in this subsection.

First, the matrix formed by J_d and R_d , that is, $A_d = J_d - R_d$, needs to be Hurwitz. A physical system in a port-Hamiltonian form is represented by the interconnection and damping matrices; since J_d is the desired interconnection matrix and R_d is the desired damping matrix, the designer could use their insight to select suitable matrices for the system. For the proposed telescope model, the matrix $J - R$ is not Hurwitz. In order to make it Hurwitz, we could choose $J_d = J$ and R_d as:

$$R_d = \begin{bmatrix} 0 & 0 & 0 & 0 \\ 0 & 0 & 0 & 0 \\ 0 & 0 & R_3 & 0 \\ 0 & 0 & 0 & R_4 \end{bmatrix}. \tag{48}$$

This selection is based on the general form of a physical system with damping depending on the angular velocity, for example, a pendulum. For the proposed telescope, the elements R_3 and R_4 of the matrix R_d of Theorem 2, when R_d is substituted in (11), multiply the angular velocity of the links ($\frac{\partial \mathcal{H}}{\partial p_1}, \frac{\partial \mathcal{H}}{\partial p_2}$).

The matrix $A_d = J_d - R_d$ is written as:

$$A_d = \begin{bmatrix} 0 & 0 & 1 & 0 \\ 0 & 0 & 0 & 1 \\ -1 & 0 & -R_3 & 0 \\ 0 & -1 & 0 & -R_4 \end{bmatrix}. \tag{49}$$

By using the Lyapunov equation $PA_d + A_d^T P = -Q$, we can demonstrate that the matrix (49) is Hurwitz if for every positive definite symmetric matrix Q , there exists a positive definite symmetric matrix P that satisfies the Lyapunov equation [22]. We start by choosing Q as the identity matrix, then, solving the Lyapunov equation for P , we obtain the solution:

$$P = \begin{bmatrix} \frac{R_3^2+2}{2R_3} & 0 & \frac{1}{2} & 0 \\ 0 & \frac{R_4^2+2}{2R_4} & 0 & \frac{1}{2} \\ \frac{1}{2} & 0 & \frac{1}{R_3} & 0 \\ 0 & \frac{1}{2} & 0 & \frac{1}{R_4} \end{bmatrix}. \tag{50}$$

The solution P is positive definite for R_3 and $R_4 > 0$; therefore, matrix A_d is Hurwitz for those values of R_3 and R_4 .

Now that the condition of A_d being Hurwitz is fulfilled, we may obtain the annihilator g^\perp . This annihilator g^\perp of g (46) needs to satisfy the condition $g^\perp g = 0$, then one possible choice is the following matrix g^\perp :

$$g^\perp = \begin{bmatrix} 1 & 0 & 0 & 0 \\ 0 & 1 & 0 & 0 \end{bmatrix}, \tag{51}$$

with the annihilator g^\perp (51) and A_d (49); we try to solve the matching Equation (8) for $\mathcal{H}_d = \mathcal{H} + \mathcal{H}_a$, which leads to:

$$\begin{aligned} \frac{\partial \mathcal{H}}{\partial p_1} &= \frac{\partial \mathcal{H}}{\partial p_1} + \frac{\partial \mathcal{H}_a}{\partial p_1}, \\ \frac{\partial \mathcal{H}}{\partial p_2} &= \frac{\partial \mathcal{H}}{\partial p_2} + \frac{\partial \mathcal{H}_a}{\partial p_2}, \end{aligned} \tag{52}$$

which can be reduced to the following equation system:

$$\frac{\partial \mathcal{H}_a}{\partial p_1} = 0, \quad \frac{\partial \mathcal{H}_a}{\partial p_2} = 0. \tag{53}$$

Therefore, the solution of (53) is:

$$\mathcal{H}_a = f(q_1, q_2), \tag{54}$$

where the term $f(q)$ can be any smooth function and is usually chosen as a quadratic function, for example, $f(q) = \frac{1}{2}K(q - L)^2$. Therefore, we define \mathcal{H}_a as:

$$\mathcal{H}_a = \frac{1}{2}K(q - L)^2, \tag{55}$$

leading to the following desired Hamiltonian \mathcal{H}_d :

$$\mathcal{H}_d = \mathcal{H} + \frac{1}{2}K(q - L)^2. \tag{56}$$

As stated in Section 2.1, L must be assigned such that condition (9) is satisfied, but before computing L , it is important to define the feasible trajectories (x^*) that the telescope could track. From open-loop Equation (45), we can replace the states x by the desired trajectories x^* and solve for u , resulting in:

$$\begin{bmatrix} u_1^* \\ u_2^* \end{bmatrix} = \frac{d}{dt} \left(D(x_1^*, x_2^*) \begin{bmatrix} x_3^* \\ x_4^* \end{bmatrix} \right) - \begin{bmatrix} 0 \\ \frac{\partial \mathcal{H}}{\partial x_2} |_{x^*} \end{bmatrix}. \tag{57}$$

The trajectories $x_1^* = \phi$ and $x_2^* = \theta$ are computed in Section 3.6 and are defined in the intervals $x_1^* \in [0^\circ, 360^\circ]$ and $x_2^* \in [0^\circ, 90^\circ]$ (0° represents an observation towards the horizon and 90° towards the zenith). There are two cases where the trajectories or their derivatives are not defined and depend on certain combinations of the observer’s latitude ($\alpha \in [-90^\circ, 90^\circ]$) and a star’s declination ($\delta \in [-90^\circ, 90^\circ]$). One case is where the observer is at one of the Earth’s poles ($\alpha = 90^\circ$ or $\alpha = -90^\circ$) and $\delta = 90^\circ$, leading to an indeterminacy, a position where the observer is aligned with the Earth’s axis rotation and the observed star is at the zenith ($\theta = 90^\circ$). In those conditions, ϕ could have any value and the observed star would still be kept in sight. The other case is for an observer in $\alpha = 0$ observing a star with $\delta = 0$; the angle q_2 has an abrupt change in its velocity when the star reaches its highest point in the sky. Aside from those cases, the positions (x_1^*, x_2^*) and their derivatives $(\dot{x}_3^*, \dot{x}_4^*)$ are defined; furthermore, in such local intervals, those functions are smooth. On the other hand, the matrix $D(q)$ (32), its time derivative and $\frac{\partial \mathcal{H}}{\partial x_2}$ are defined for $q_1 \in [0, 360^\circ]$ and $q_2 \in [0^\circ, 90^\circ]$. Then, the right-hand side of Equation (57) is defined for all the trajectories, with the exception of the mentioned cases.

Now we can compute L for the mentioned feasible trajectories. For the case of a feasible trajectory x^* , substituting (56) into (9), results in the following equation:

$$\frac{d}{dt} \left(D(x_1^*, x_2^*) \begin{bmatrix} \dot{x}_3^* \\ \dot{x}_4^* \end{bmatrix} \right) = \begin{bmatrix} -R_3 \dot{x}_3^* - \frac{\partial(\mathcal{H} + \frac{1}{2}K(q-L)^2)}{\partial q_1} |_{x^*} \\ -R_4 \dot{x}_4^* - \frac{\partial(\mathcal{H} + \frac{1}{2}K(q-L)^2)}{\partial q_2} |_{x^*} \end{bmatrix}. \tag{58}$$

Equation (58) is solved for L , so we can substitute the L solution into Equation (56) to obtain the desired Hamiltonian \mathcal{H}_d ; since the result is rather cumbersome, it is not displayed but directly substituted into Equation (10) (u) to obtain the following control law:

$$u = \begin{bmatrix} -R_3 \dot{q}_1 - \frac{K(2q_1 - \frac{\sigma_1}{K})}{2} \\ -R_4 \dot{q}_2 - \frac{K(2q_2 - \frac{\sigma_2}{50K})}{2} \end{bmatrix}, \tag{59}$$

where

$$\begin{aligned} \sigma_1 &= 2(I_{12} \dot{x}_3^* + I_{21} \dot{x}_3^* + R_3 x_3^* + K x_1^* - I_{21} \dot{x}_3^* \cos(x_2^*))^2 + I_{22} \dot{x}_3^* \cos(x_2^*)^2 \\ &\quad + B_2^2 \dot{x}_3^* m_2 + \dot{x}_3^* l_1^2 m_2 + \dot{x}_3^* l_{cm1}^2 m_1 + \dot{x}_3^* l_{cm2}^2 m_2 \cos(x_2^*)^2 \\ &\quad + I_{21} x_3^* x_4^* \sin(2x_2^*) - I_{22} x_3^* x_4^* \sin(2x_2^*) + 2 B_2 \dot{x}_3^* l_1 m_2 - B_2 x_4^{*2} l_{cm2} m_2 \cos(x_2^*) \\ &\quad - x_4^{*2} l_1 l_{cm2} m_2 \cos(x_2^*) - x_3^* x_4^* l_{cm2}^2 m_2 \sin(2x_2^*) - B_2 \dot{x}_4^* l_{cm2} m_2 \sin(x_2^*) \\ &\quad - x_4^* l_1 l_{cm2} m_2 \sin(x_2^*), \\ \sigma_2 &= 100 I_{23} \dot{x}_4^* + 100 R_4 x_4^* + 100 K x_2^* + 981 l_{cm2} m_2 \cos(x_2^*) - 50 I_{21} x_3^{*2} \sin(2x_2^*) \\ &\quad + 50 I_{22} x_3^{*2} \sin(2x_2^*) + 100 \dot{x}_4^* l_{cm2}^2 m_2 + 50 x_3^{*2} l_{cm2}^2 m_2 \sin(2x_2^*) \\ &\quad - 100 B_2 \dot{x}_3^* l_{cm2} m_2 \sin(x_2^*) - 100 \dot{x}_3^* l_1 l_{cm2} m_2 \sin(x_2^*). \end{aligned}$$

Notice that σ_1 and σ_2 depend on the constant parameters of the telescope (mass, inertia, length of the links) and are functions of the trajectories (x_1^*, x_2^*) and velocities $(\dot{x}_3^*, \dot{x}_4^*)$. Also, since the state variables in the PCH model are q and p , in this case, the variables \dot{q}_1 and \dot{q}_2 are considered functions of the independent variables q and p , with relation (41).

The control law (59) is going to be applied to the PCH model (47) and compared to the inverse-dynamics control and super-twisting control computed in the following subsections. The PCH model (47) and its controller in general form (10) are shown in Figure 4 as a block diagram. Note that for the proposed telescope case J, R and g are constant and do not appear as a function of x . The term \mathcal{H}_d in (10) (and in the diagram) is defined in (56) and comprises two terms, \mathcal{H} (43) and \mathcal{H}_a (55). Also, although L (a term

in \mathcal{H}_a) is not shown explicitly, it is a function of the trajectories $[\phi, \theta]^\top$ and their time derivatives.

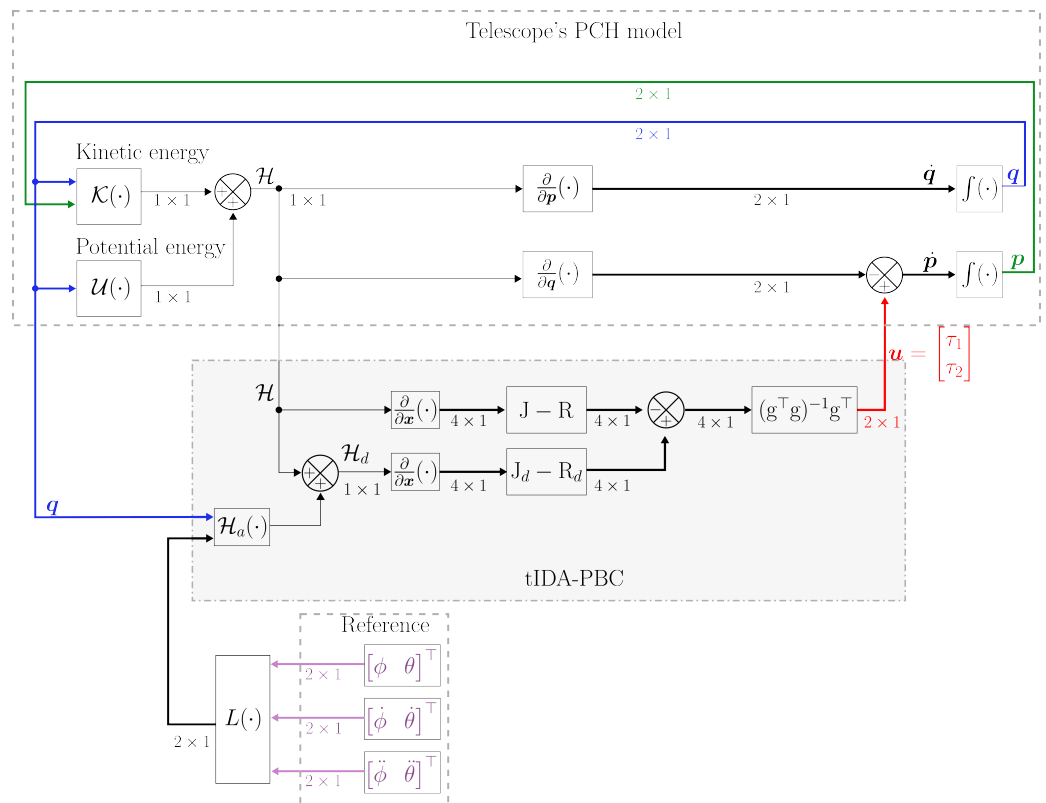


Figure 4. Block diagram of the telescope’s PCH model and its controller (tIDA-PBC) for the trajectories $[\phi, \theta]^\top$.

Remark 1. Notice that we avoided the explicit cumbersome representation of large expressions such as \mathcal{H}_a , \mathcal{H}_d , L or $D^{-1}(x)$ to try to enhance the readability in this work. The control law (59) is an exception since we were aiming to obtain it and it is in the final part of its subsection; furthermore, the lengthy part (σ_1 and σ_2) depends on the constant inertias, masses and the position references with their derivatives; in contrast, the state variables and gains are represented in a compact form.

3.3. Inverse-Dynamics Control (IDC)

For the inverse-dynamics control, we need to find a nonlinear feedback control law $u = f(q, \dot{q})$, such that when substituted in (35), it results in a linear closed-loop system. For the case of manipulator dynamics Equation (35), this is achieved by choosing $u = \tau$ as:

$$u = D(q)a_q + C(q, \dot{q}) + g(q). \tag{60}$$

Since the matrix $D(q)$ is invertible for this kind of system, the substitution of (60) in (35) leads to:

$$\ddot{q} = a_q. \tag{61}$$

Now the system under control (60) is linear and decoupled with respect to the new input a_q . Hence, a_q can be designed to control a linear second-order system and a natural choice is the following equation

$$a_q = -K^0(q - q_d) - K^1(\dot{q} - \dot{q}_d) + \ddot{q}_d. \tag{62}$$

That is because it leads to the homogeneous second-order differential equation:

$$(\ddot{q} - \ddot{q}_d) + K^1(\dot{q} - \dot{q}_d) + K^0(q - q_d) = 0, \tag{63}$$

where K^0 and K^1 are 2×2 diagonal gain matrices and q_d is the desired position (angles ϕ and θ) (83) which will be described in Section 3.6). The characteristic equation of the closed-loop system (63) for the i -link is written as follows:

$$s^2 + K_i^1 s + K_i^0 = 0, \tag{64}$$

where K_i^1 (K_i^0) is the i -th element of the diagonal matrix K^1 (K^0) and its stability is analyzed via the following proposition:

Proposition 2. *Polynomial (64) is the characteristic function of closed-loop system (63). If $K_i^0, K_i^1 > 0$ in polynomial (64), then all its roots are in the left half of the s -plane; therefore, the closed-loop system (63) is stable.*

Proof of Proposition 2. We use the Routh–Hurwitz criterion to identify the stable poles in the closed-loop system (63) from its characteristic Equation (64). First, we generate the Routh array of coefficients, which leads to:

$$\begin{array}{ccc} s^2 & 1 & K_i^0 \\ s^1 & K_i^1 & 0 \\ s^0 & K_i^0 & \end{array} . \tag{65}$$

The Routh–Hurwitz criterion declares that the number of roots of the polynomial that are in the right half of the s -plane is equal to the number of sign changes in the first column of the Routh array of coefficients (65) [28]. Hence, for $K_i^0, K_i^1 > 0$, there are no sign changes and all the poles of the closed-loop system (63) are in the left half of the s -plane, making it stable. □

We can also choose $K^0 = \text{diag}(\omega_1^2, \omega_2^2)$ and $K^1 = \text{diag}(2\omega_1, 2\omega_2)$ with $\omega_i > 0$, so each link, in addition to being stable, also has the response of a critically damped linear second-order system with natural frequency ω_i .

For a more detailed lecture on inverse-dynamics control, the interested reader is referred to [5,6], as this control is not the main focus of this work.

3.4. Super-Twisting Control Combined with Non-Linear Block Control (NBC-STSM)

In order to apply the super-twisting control algorithm explained in Section 2.2, the state–space representation of the two-degrees-of-freedom telescope model (38) is transformed to the NBC form (14). For this, in system (38) the two following blocks ($r = 2$) $x_1 = [x_1 \ x_2]^T$ and $x_2 = [x_3 \ x_4]^T$ are defined as follows:

$$\begin{aligned} \dot{x}_1 &= x_2 \\ \dot{x}_2 &= f(x_1, x_2) + B(x_1)u, \end{aligned} \tag{66}$$

where $f(x_1, x_2) = -[D^{-1}(x_1)][C(x_1, x_2)x_2 + g(x_2)]$, $B(x_1) = [D^{-1}(x_1)]$, $u = [\tau_1 \ \tau_2]^T$. Then, applying the procedure for transforming system (66) to the block control form, the resulting system is:

$$\begin{aligned} \dot{z}_1 &= -k_1 z_1 + E_1 z_2 \\ \dot{z}_2 &= \bar{f}_2(z, x_{1d}, \dot{x}_{1d}, t) + \bar{E}_2 u, \end{aligned} \tag{67}$$

where the sliding manifold $s_2 = z_2$ is defined from system (67). For simplicity, the procedure for transforming system (66) to the block control form (67) is not included here. This is due to this transformation not being the main scope of this work. The reader is kindly

referred to [25] for information on the procedure of transformation. Now, it is possible to use the super-twisting algorithm as follows:

$$v_{si} = \lambda_i |s_i|^{\frac{1}{2}} \text{sign } s_i + v_{s1i}, \tag{68}$$

where $\dot{v}_{si} = \alpha_i \text{sign } s_i$, $\lambda_i = \begin{bmatrix} \lambda_{q1} & 0 \\ 0 & \lambda_{q2} \end{bmatrix}$ and $\alpha_i = \begin{bmatrix} \alpha_{q1} & 0 \\ 0 & \alpha_{q2} \end{bmatrix}$.

$$\begin{aligned} \dot{s}_i &= F_i(\lambda_{r,i}, \epsilon_{1,i}, s_i) - B_{2i} \left(\lambda_i |s_i|^{\frac{1}{2}} \text{sign}_i s + v_{s1,i} \right), \\ \dot{v}_{s,i} &= \alpha_i \text{sign } s_i. \end{aligned} \tag{69}$$

Proposition 3. For some $\lambda_i > 2\Delta_i$ and $\alpha_i > \frac{1}{2} \frac{\lambda_i^2 (\Delta_i - \lambda_i)}{\lambda_i - 2\Delta_i}$, there exists an instant time t such that the solution of system (14) (and particularly of z_1) presents an asymptotic movement to zero.

Proof of Proposition 3. This follows the procedure described in [29]. As each degree of freedom of the state-space model of telescope (38) is comprised of its corresponding control inputs ($u_1 = \tau_1$ and $u_2 = \tau_2$) and outputs ($x_1 = q_1$ and $x_2 = q_2$), respectively, it is possible to represent system (69) in scalar form as:

$$\begin{aligned} \dot{s}_i &= -k_{1i} |s_i|^{\frac{1}{2}} \text{sign}(s_i) + u_i + \varphi_i, \\ \dot{u}_i &= -k_{2i} \text{sign}(s_i), \quad i = q_1, q_2, \end{aligned} \tag{70}$$

where it is defined that:

$$[k_{1q1} \quad k_{1q2}]^\top = B_2 \lambda_i, \quad [k_{2q1} \quad k_{2q2}]^\top = B_2 \alpha_i, \quad [u_1 \quad u_2]^\top = B_2 v_{s1}. \tag{71}$$

Then, by using the procedure presented in [26], the following is proposed:

$$\zeta_i = \begin{bmatrix} |s_i|^{\frac{1}{2}} \text{sign}(s_i) \\ u_i \end{bmatrix}, \quad \text{with } |\zeta_{1i}| = |s_i|^{\frac{1}{2}}, \tag{72}$$

and:

$$\dot{\zeta}_i = \frac{1}{|\zeta_{1i}|} \begin{bmatrix} \frac{1}{2} (-k_{1i} \zeta_{1i} + \zeta_{2i} + \varphi_i) \\ -k_{2i} \zeta_{1i} \end{bmatrix}. \tag{73}$$

Notice that Equation (73) can be expressed as the following linear system:

$$\dot{\zeta}_i = A_i \zeta_i + \rho_i, \tag{74}$$

where:

$$\begin{bmatrix} \dot{\zeta}_{1i} \\ \dot{\zeta}_{2i} \end{bmatrix} = \frac{1}{|\zeta_{1i}|} \begin{bmatrix} -\frac{k_{1i}}{2} & \frac{1}{2} \\ -k_{2i} & 0 \end{bmatrix} \begin{bmatrix} \zeta_{1i} \\ \zeta_{2i} \end{bmatrix} + \begin{bmatrix} \frac{1}{2|\zeta_{1i}|} \varphi_i \\ 0 \end{bmatrix}, \tag{75}$$

where the function φ_i is bounded with the following restrictions [26]:

$$|\varphi_i| \leq \Delta_i |s_i|^{\frac{1}{2}}, \quad |\varphi_i| \leq \Delta_i |\zeta_{1i}|, \quad \Delta_i \geq 0, \tag{76}$$

and for our specific application:

$$\varphi_i = \Delta_i |s_i|^{\frac{1}{2}} \text{sign}(s_i) = \Delta_i \zeta_{1i}. \tag{77}$$

Then, to analyze the stability condition of system (75), the following Lyapunov function candidate is proposed [29]:

$$V_i(\zeta) = \zeta_i^\top P_i \zeta_i, \tag{78}$$

where

$$P_i = \frac{1}{2} \begin{bmatrix} 4k_{2i} + k_{1i}^2 & -k_{1i} \\ -k_{1i} & 2 \end{bmatrix}.$$

The derivative of (78) is:

$$\dot{V}_i(\zeta_i) = \zeta_i^T (A_i^T P_i + P_i A_i) \zeta_i + 2\zeta_i^T P_i \rho_i. \tag{79}$$

Involving the restriction of function f_i (77) in the term ρ_i of (79) yields:

$$\dot{V}_i(\zeta_i) = -\frac{1}{|\zeta_{1i}|} \zeta_i^T Q_i \zeta_i, \tag{80}$$

where

$$Q_i = \frac{k_{1i}}{2} \begin{bmatrix} k_{1i}^2 + 2k_{2i} - \Delta_i \left(k_{1i} + 4\frac{k_{2i}}{k_{1i}} \right) & -k_{1i} \\ -(k_{1i} - \delta_i) & 1 \end{bmatrix}.$$

The matrix Q_i must be positive definite; then, $k_{1i} = \lambda_i$ and $k_{2i} = \alpha_i$ and the values should fulfill the following conditions:

$$\begin{aligned} \lambda_i &> 2\Delta_i, \\ \alpha_i &> \frac{1}{2} \frac{\lambda_i^2 (\Delta_i - \lambda_i)}{\lambda_i - 2\Delta_i}. \end{aligned} \tag{81}$$

Then, the derivative of the Lyapunov function (80) is negative definite and asymptotic stability is ensured with the restrictions (81) [30]. Thus, an asymptotic movement of the tracking error variable z_1 is presented. □

3.5. Liquid-Mirror Control

A telescope can be described by its aperture and ϵ -number, where the aperture is the clear diameter of the main lens or mirror. The ϵ number is the ratio between the focal length (distance from the main lens or mirror to the point where parallel light rays will meet) of the main lens or mirror and the aperture. These values are important because the characteristics such as brightness, size and clarity of the image produced by a telescope depend on both the aperture and the focal length [31]. For the liquid mirror, the aperture depends on the size of its container, but the focal length can be adjusted. As stated in [3], a rotating fluid’s surface takes the shape of a parabola and if the fluid reflects, it could be used as the primary mirror of a telescope. For a liquid mirror in a container, the relation between its focal length (L), the acceleration of gravity g and the angular velocity of the container ω is described by [2]:

$$L = \frac{g}{2\omega^2}. \tag{82}$$

The focal length of a liquid mirror remains constant for a constant velocity ω , so it is necessary to apply a control strategy to the motor that keeps rotating the base of the liquid-mirror container. This work focuses on the tracking of a star by the proposed telescope assuming that the liquid mirror is kept at a constant velocity, but a candidate control to regulate the liquid mirror’s angular velocity, for future implementation, is the state feedback linearization technique applied to a DC motor model, as described in [32].

3.6. Star’s Position

The proposed liquid-mirror telescope has the capacity to track an arbitrary star’s trajectory. As this telescope is in alt-azimuth configuration, the position of the star is represented in horizon coordinates (azimuth ϕ and altitude θ) computed from the star’s declination (δ), the hour angle (H) and the observer’s geographical latitude (α). The

relationship between the star’s coordinates, the observer’s geographical latitude and the horizon coordinates is computed from a modified version presented in [33] as:

$$\begin{aligned} \tan \phi &= \frac{\sin \lambda \sin H}{\cos \alpha \cos \lambda - \sin \alpha \sin \lambda \cos H} , \\ \sin \theta &= \cos \alpha \sin \lambda \cos H + \sin \alpha \cos \lambda , \end{aligned} \tag{83}$$

where the celestial colatitude of the star $\lambda = 90^\circ - \delta$. Figure 5 shows one half of the celestial sphere, with an observer positioned at O ; the position of a star is indicated by P_s . It can be seen that the azimuth ϕ increases in the positive direction about the local vertical (z axis), that is, in the sense NWSE (the letters refer to north, west, south and east) with respect to the star’s projection on the horizon at B . The altitude (θ) increases from the horizon and it is the angle subtended at O by the points B and P_s ; a negative θ indicates that the observed object is below the horizon. It is important to remark that the angles ϕ and θ of (83) constitute the reference signals to be tracked by the angular positions of the orientation of the telescope q_1 and q_2 of (29), respectively.

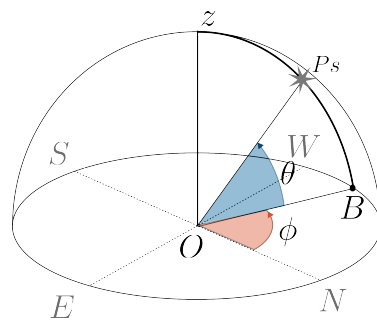


Figure 5. Horizon coordinates of a celestial body.

3.7. Simulation Results

The following simulations were done using MATLAB® and SIMULINK®, with a fixed-step, solver ode4 (Runge–Kutta) and step size of 1 ms. These simulations show the tracking of the star *Regulus*, from the constellation *Leo* over four hours on 1 March 2023 at 22:00 h, considering that the observer’s coordinates are those of the *Centro Universitario de los Lagos, Universidad de Guadalajara* (latitude = 21.357098° and longitude = −101.951965°) located in Mexico. The two coordinates to track by the proposed telescope are the angles ϕ and θ obtained from (83), which correspond to the trajectory of the star *Regulus*. This trajectory is presented in Figure 6.

A comparison is made between the three presented controllers: Port-Hamilton Control (PCH), Inverse-Dynamics Control (IDC) and Non-linear block controllable form combined with the Super-Twisting Sliding-Mode control (NBC-STSM). Then, the comparison consists of showing the tracking performance for each reference ϕ and θ , the tracking errors and the torques exerted by using each one of the controllers. Also, the root-mean-square (RMS) error of all the controllers in the steady-state is obtained, considering the response as steady when it is within 1% of the reference magnitude. The simulations are made without considering external perturbations since the telescope is considered to operate under a restricted scenario free of big disturbances.

Figures 7 and 8 show the tracking performance of the angles q_1 and q_2 with the references ϕ and θ , respectively, of the star *Regulus*, obtained from (83), using each one of the controllers PCH, IDC and NBC-STSM. Also, a detail of ten seconds is added in both figures to visualize the transitory responses. All the controllers have a good performance reaching the reference at similar times and maintaining the tracking in the absence of disturbances.

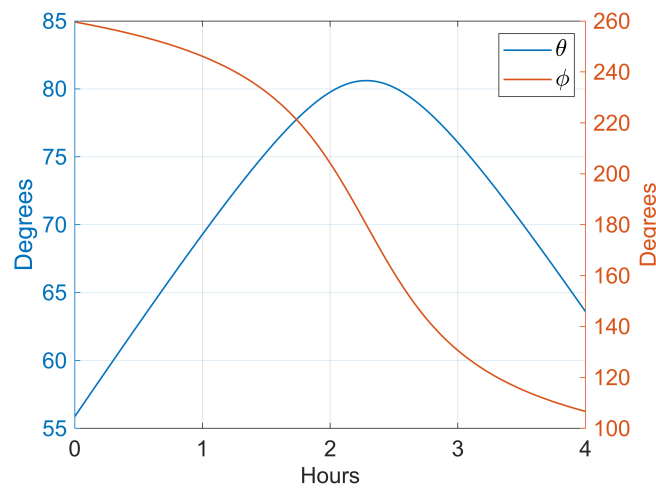


Figure 6. Coordinates of *Regulus* for an observer at the *Centro Universitario de los Lagos* from 22:00 h to 02:00 h.

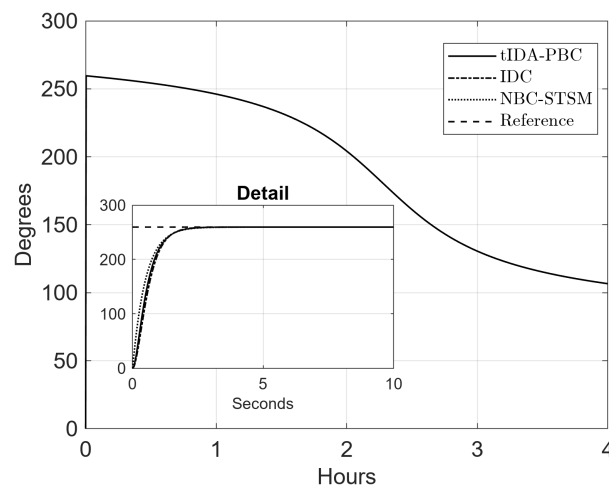


Figure 7. Tracking performance of the angle q_1 with the reference ϕ of the star *Regulus*, using each one of the controllers PCH, IDC and NBC-STSM.

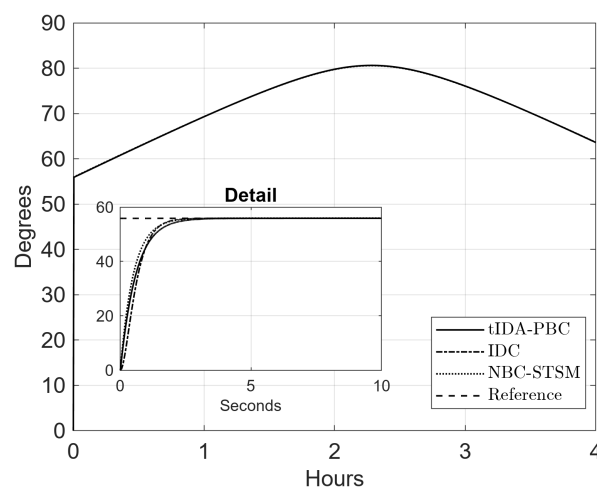


Figure 8. Tracking performance of the angle q_2 with the reference θ of the star *Regulus* using each one of the controllers PCH, IDC and NBC-STSM.

Figures 9 and 10 show the tracking errors $\phi - q_{1i}$ and $\theta - q_{2i}$, respectively, with $i = 1, 2, 3$; 1 to PCH, 2 to IDC and 3 to NBC-STSM. The error is decreased at similar times with all the controllers and it remains stable. Table 2 contains the RMS error for angles q_1

and q_2 and it is added as a complement to the comparison, showing that, although there are similar responses in the transitory, the RMS errors of the PCH and IDC are smaller than the NBC-STSM in steady state. For a better comparison of the responses of systems, we consider the steady state when defining the settling time $t_s = 1\%$ criterion.

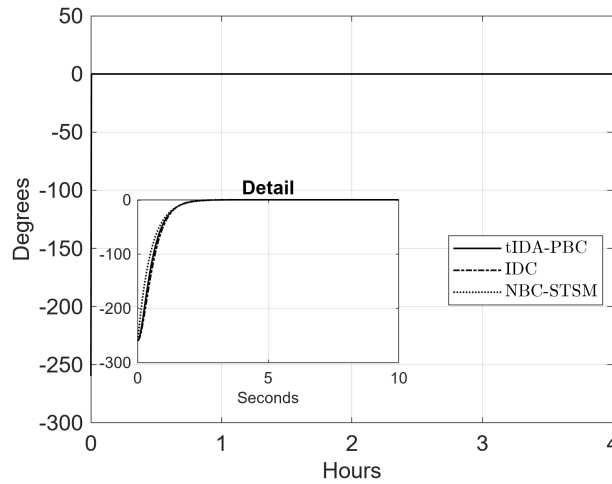


Figure 9. Tracking errors $\phi - q_{1i}$, with $i = 1, 2, 3$; 1 to PCH, 2 to IDC and 3 to NBC-STSM.

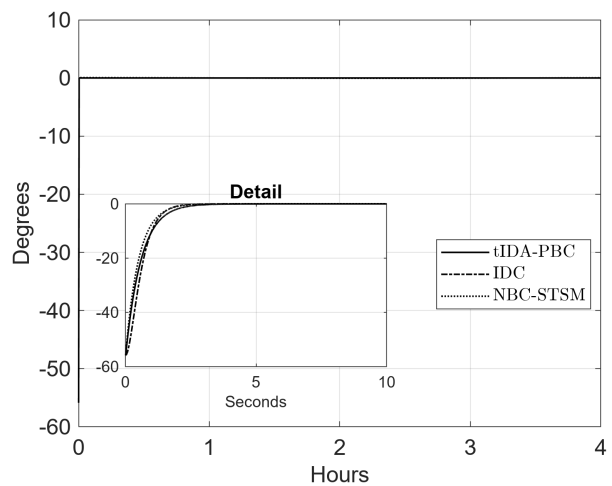


Figure 10. Tracking errors $\theta - q_{2i}$, with $i = 1, 2, 3$; 1 to PCH, 2 to IDC and 3 to NBC-STSM.

Table 2. Comparison between the settling time and RMS errors of each controller for the angles q_1 and q_2 .

Angle	Parameter	Controller		
		PCH	IDC	NBC-STSM
q_1	RMS error (deg)	0.0083	0.0055	0.0108
	Settling time (s)	2.2150	2.1140	2.3030
q_2	RMS error (deg)	0.0025	0.0004	0.0312
	Settling time (s)	2.6890	2.1140	2.2430

Figures 11 and 12 show the torques u_1 and u_2 needed for the controllers PCH, IDC and NMB-STSM in order to drive the angular positions q_1 and q_2 to the references ϕ and θ , respectively. Resembling the behavior of the tracking performance of the angular positions for each controller, the torque values are very close in both the transient and steady states. The exception is the torque value for the NBC-STSM that adjusts q_2 ; its difference compared with the torques of PCH and IDC can be seen in Figure 12 and the corresponding RMS error in the tracking shown in Table 2, being bigger than PCH and IDC RMS errors.

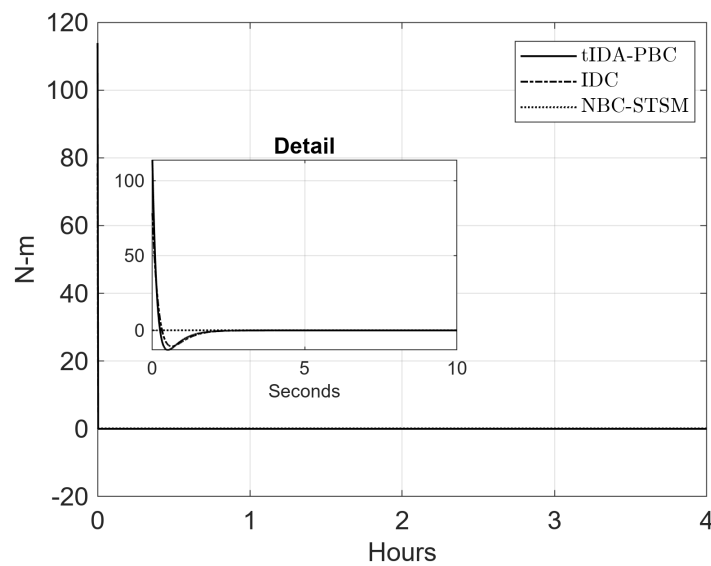


Figure 11. Torque values u_1 needed for the controllers PCH, IDC and NMB-STSM in order to drive the angular position q_1 to the reference ϕ .

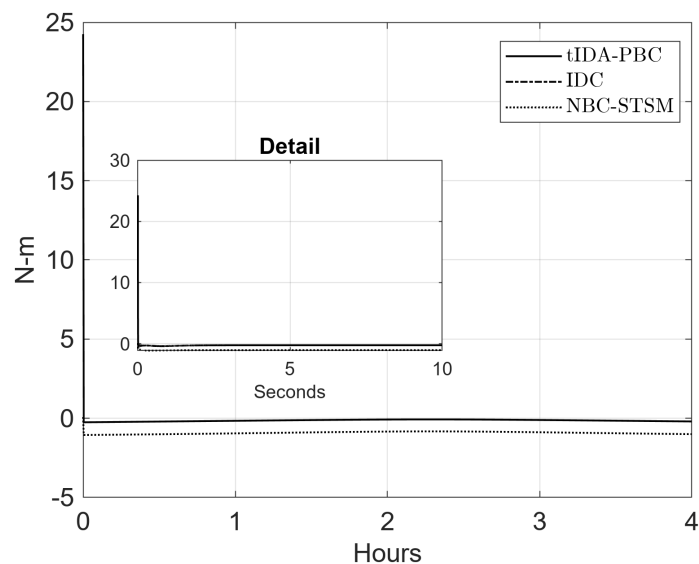


Figure 12. Torque values u_2 needed for the controllers PCH, IDC and NMB-STSM in order to drive the angular position q_2 to the reference θ .

In order to see the robustness of each controller, an external disturbance with a magnitude 5 N·m is applied, starting at 10 s and vanishing at 20 s. Figures 13 and 14 show the first 30 s of the *Regulus* star tracking to each link of the telescope, respectively, and where the external disturbance effect is depicted. As we can see from both figures when the disturbance appears, all of the angular positions of each controller deviate from the reference, but, due to its robustness, the NBC-STSM tracks the reference again for the duration of the perturbation. Although the IDC has the smaller RMS error, we can see that it is the most sensitive to disturbances, deviating from the reference more than the NBC-STSM and tIDA-PBC, especially for q_2 . On the other hand, the tIDA-PBC deviates the least under the presence of external disturbances and it has a smaller RMS error than the NBC-STSM, showing a good performance under the presence of external vanishing disturbances.

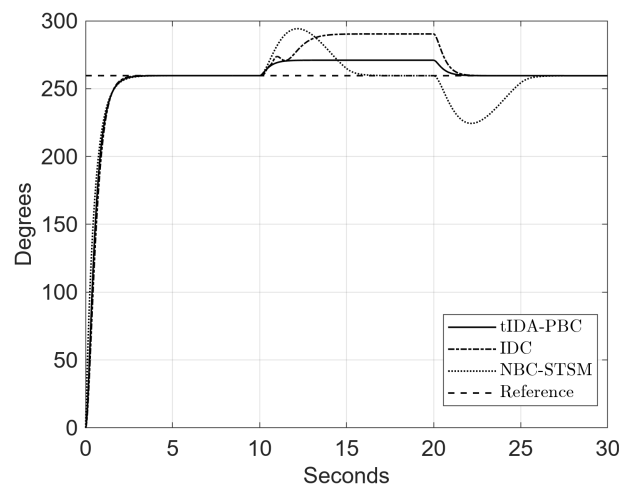


Figure 13. Tracking performance of the angle q_1 with the reference ϕ of the star *Regulus* under a vanishing disturbance.

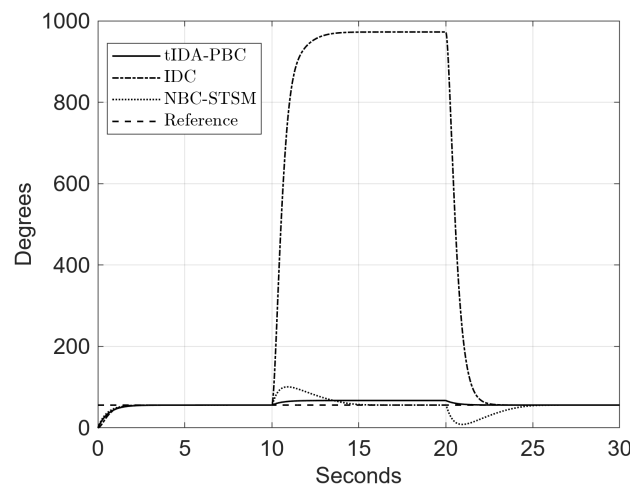


Figure 14. Tracking performance of the angle q_2 with the reference θ of the star *Regulus* under a vanishing disturbance.

4. Conclusions

The three controllers (IDC, NBC-STSM and tIDA-PBC) have a good performance when tracking an object in the absence of perturbations. The IDC has great accuracy but the parameters of the system have to be known exactly; therefore, it is not robust to any disturbance or parametric variations. The NBC-STSM is very robust to external and continuous disturbances; it rejects them and maintains good tracking of the reference. The tIDA-PBC strategy does not rely on the cancellation of nonlinearities as the IDC; it rather exploits the energy properties of the system, resulting in a more robust system. Although it does not reject non-vanishing external disturbances, it has more robustness to those than the IDC; that is, the offset with the reference due to the disturbances is smaller; furthermore, it ensures robustness against frictions and it has some robustness against parametric variations. Hence, for the considered conditions in which the telescope may operate, a reasonably good dynamical model with some unmodeled frictions and occasional vanishing disturbances due to wind, the tIDA-PBC may ensure a smooth, steady tracking, allowing even for astrophotography while tracking a star.

With respect to the results, since the simulations of the tIDA-PBC showed good behavior for star tracking and its characteristics are suited for the conditions in which a telescope could operate, we consider that the next step in extending this work is the construction of the proposed telescope. Therefore, we could have a real-time implementation of the tIDA-PBC. Such an implementation, aside from testing the controller, will allow us to test

the proposed liquid-mirror telescope and compare not only the tracking but the quality of the image with a conventional telescope of similar size.

Author Contributions: Methodology, J.C.A.T. and C.E.C.; Validation, P.E.; Formal analysis, C.E.C. and H.V.R.; Investigation, J.C.A.T.; Writing—review & editing, P.E.; Supervision, H.V.R. All authors have read and agreed to the published version of the manuscript.

Funding: The authors thank CONAHCYT (México) under the program *Estancias posdoctorales por México 2022* with respect to scholarship number 779292, PROSNI and SNCA 2023 II (DCET) under project no. 271276.

Data Availability Statement: Not applicable.

Conflicts of Interest: The authors declare no conflict of interest.

References

- Hickson, P.; Pfrommer, T.; Cabanac, R.; Crotts, A.; Johnson, B.; De Lapparent, V.; Lanzetta, K.M.; Gromoll, S.; Mulrooney, M.K.; Sivanandam, S.; et al. The Large Zenith Telescope: A 6 m Liquid-Mirror Telescope. *Publ. Astron. Soc. Pac.* **2007**, *119*, 444. [[CrossRef](#)]
- Borra, E.F. The liquid-mirror telescope as a viable astronomical tool. *J. R. Astron. Soc. Can.* **1982**, *76*, 245–256.
- Borra, E.F. Liquid mirrors. *Can. J. Phys.* **1995**, *73*, 109–125. [[CrossRef](#)]
- Surdej, J.; Hickson, P.; Borra, H.; Swings, J.P.; Habraken, S.; Akhunov, T.; Bartczak, P.; Chand, H.; De Becker, M.; Delchambre, L.; et al. The 4-m international liquid-mirror telescope. *Bull. Soc. R. Sci. Liege* **2018**, *87*, 68–79. [[CrossRef](#)]
- Spong, M.W.; Hutchinson, S.; Vidyasagar, M. *Robot Modeling and Control*; John Wiley & Sons: Hoboken, NJ, USA, 2020.
- Sciavicco, L.; Siciliano, B. *Modelling and Control of Robot Manipulators*; Springer Science & Business Media: Berlin, Germany, 2001.
- Utkin, V.; Guldner, J.; Shi, J. *Sliding Mode Control in Electro-Mechanical Systems*; CRC Press: Boca Raton, FL, USA, 2017.
- Perruquetti, W.; Barbot, J.P. *Sliding Mode Control in Engineering*; Marcel Dekker: New York, NY, USA, 2002; Volume 11.
- Liu, J.; Shen, X.; Alcaide, A.M.; Yin, Y.; Leon, J.I.; Vazquez, S.; Wu, L.; Franquelo, L.G. Sliding-mode control of grid-connected neutral-point-clamped converters via high-gain observer. *IEEE Trans. Ind. Electron.* **2021**, *69*, 4010–4021. [[CrossRef](#)]
- Wang, T.; Wang, B.; Yu, Y.; Xu, D. Fast High-Order Terminal Sliding-Mode Current Controller for Disturbance Compensation and Rapid Convergence in Induction Motor Drives. *IEEE Trans. Power Electron.* **2023**, *38*, 9593–9605. [[CrossRef](#)]
- Wang, B.; Wang, T.; Yu, Y.; Xu, D. Second-Order Terminal Sliding-Mode Speed Controller for Induction Motor Drives with Nonlinear Control Gain. *IEEE Trans. Ind. Electron.* **2022**, *70*, 10923–10934. [[CrossRef](#)]
- Swikir, A.; Utkin, V. Chattering analysis of conventional and super twisting sliding mode control algorithm. In Proceedings of the 2016 14th International Workshop on Variable Structure Systems (VSS), Nanjing, China, 1–4 June 2016; pp. 98–102.
- Ortega, R.; García-Canseco, E. Interconnection and Damping Assignment Passivity-Based Control: A Survey. *Eur. J. Control* **2004**, *10*, 432–450. [[CrossRef](#)]
- Duindam, V.; Macchelli, A.; Stramigioli, S.; Bruyninckx, H. *Modeling and Control of Complex Physical Systems the Port-Hamiltonian Approach*; Springer: London, UK, 2009.
- Ortega, R.; Van der Schaft, A.; Maschke, B.; Escobar, G. Energy-shaping of port-controlled Hamiltonian systems by interconnection. In Proceedings of the 38th IEEE Conference on Decision and Control (Cat. No. 99CH36304), Phoenix, AZ, USA, 7–10 December 1999; Volume 2, pp. 1646–1651.
- Ortega, R.; van der Schaft, A.; Maschke, B.; Escobar, G. Interconnection and damping-assignment passivity-based control of port-controlled Hamiltonian systems. *Automatica* **2002**, *38*, 585–596. [[CrossRef](#)]
- Chi, J.; Yu, H.; Yu, J. Hybrid Tracking Control of 2-DOF SCARA Robot via Port-Controlled Hamiltonian and Backstepping. *IEEE Access* **2018**, *6*, 17354–17360. [[CrossRef](#)]
- Gómez-Estern, F.; Van der Schaft, A.J. Physical damping in IDA-PBC controlled underactuated mechanical systems. *Eur. J. Control* **2004**, *10*, 451–468. [[CrossRef](#)]
- Donaire, A.; Romero, J.G.; Ortega, R.; Siciliano, B.; Crespo, M. Robust IDA-PBC for underactuated mechanical systems subject to matched disturbances. *Int. J. Robust Nonlinear Control* **2017**, *27*, 1000–1016. [[CrossRef](#)]
- Acosta, J.Á.; Sanchez, M.; Ollero, A. Robust control of underactuated aerial manipulators via IDA-PBC. In Proceedings of the 53rd IEEE Conference on Decision and Control, Los Angeles, CA, USA, 15–17 December 2014; pp. 673–678.
- Yaghmaei, A.; Yazdanpanah, M.J. Trajectory tracking for a class of contractive port-Hamiltonian systems. *Automatica* **2017**, *83*, 331–336. [[CrossRef](#)]
- Khalil, H.K. *Nonlinear Control*; Pearson: New York, NY, USA, 2015; Volume 406.
- Shakibjoo, A.D.; Moradzadeh, M.; Moussavi, S.Z.; Mohammadzadeh, A.; Vandeveld, L. Load frequency control for multi-area power systems: A new type-2 fuzzy approach based on Levenberg–Marquardt algorithm. *ISA Trans.* **2022**, *121*, 40–52. [[CrossRef](#)] [[PubMed](#)]
- Khalil, H.K. *Nonlinear Systems*, 3rd ed.; Patience Hall: Hoboken, NJ, USA, 2002; Volume 115.
- Loukianov, A.G. Robust block decomposition sliding-mode control design. *Math. Probl. Eng.* **2003**, *8*, 349–365. [[CrossRef](#)]

26. Morfin, O.A.; Valenzuela, F.A.; Betancour, R.R.; Castañeda, C.E.; Ruiz-Cruz, R.; Valderrabano-Gonzalez, A. Real-time SOSM super-twisting combined with block control for regulating induction motor velocity. *IEEE Access* **2018**, *6*, 25898–25907. [[CrossRef](#)]
27. Goldstein, H.; Poole, C.; Safko, J. *Classical Mechanics Pearson New International Edition*; Pearson Education, Limited: London, UK, 2013; p. 660.
28. Nise, N.S. *Control Systems Engineering*; John Wiley & Sons: Hoboken, NJ, USA, 2020.
29. Dávila, A.; Moreno, J.A.; Fridman, L. Optimal Lyapunov function selection for reaching time estimation of super twisting algorithm. In Proceedings of the 48th IEEE Conference on Decision and Control (CDC) Held Jointly with 2009 28th Chinese Control Conference, Shanghai, China, 15–18 December 2009; pp. 8405–8410.
30. Garduño, O.A.M.; Cruz, R.R.; Murillo, F.A.V.; Betancour, R.R.; Hernández, C.E.C.; Téllez, F.O. Robust cascade controller for the power factor of the three-phase supply and the induction motor velocity. *ISA Trans.* **2023**. [[CrossRef](#)]
31. Moché, D.L. *Astronomy*; Wiley: Hoboken, NJ, USA, 2009.
32. Morfin, O.A.; Castañeda, C.E.; Valderrabano-Gonzalez, A.; Hernandez-Gonzalez, M.; Valenzuela, F.A. A real-time SOSM super-twisting technique for a compound DC motor velocity controller. *Energies* **2017**, *10*, 1286. [[CrossRef](#)]
33. Cristobal, J.; Tapia, A.; Castañeda, C.; Vargas-Rodríguez, H. An alternative approach for determining the motor rotation rates for an altazimuth telescope mount. In Proceedings of the Herramientas y Tecnologías Especificas Para Beneficio de las Instituciones y Comunidades, Cuernavaca, Mexico, 21–23 March 2018.

Disclaimer/Publisher’s Note: The statements, opinions and data contained in all publications are solely those of the individual author(s) and contributor(s) and not of MDPI and/or the editor(s). MDPI and/or the editor(s) disclaim responsibility for any injury to people or property resulting from any ideas, methods, instructions or products referred to in the content.